Conference on Modelling Fluid Flow (CMFF'22)
The 18th International Conference on Fluid Flow Technologies
Budapest, Hungary, August 30 -September 2, 2022

INSIGHTS INTO THE FLOW SITUATION OF A MULTI-STAGE CENTRIFUGAL PUMP

Helmut BENIGNI[1], Stefan HÖLLER[2], Bernhard LECHNER[3], Jürgen KONRAD[3], Helmut JABERG[1,2]

[1] Corresponding Author. Institute of Hydraulic Fluidmachinery, Graz University of Technology. Kopernikusgasse 24/IV, A-8010 Graz, Austria. Tel.: +43 316 873 7578, Fax: +43 316 873 107578, E-mail: helmut.benigni@tugraz.at
[2] Prof. Dr. Jaberg und Partner GmbH, Kerscheckstrasse 41, 8076 Vasoldsberg, Austria
[3] Dickow Pumpen GmbH & Co. KG, Siemensstraße 22, 84478 Waldkraiburg, Germany

ABSTRACT

The present paper analyses a multi-stage ring-section pump concerning head, efficiency, cavitation and optimisation potential and comparison with existing test bench results and systematic optimisation. The investigation was carried out within the scope of several stages. An extracted fluid volume with many details is necessary to enable the highest possible accuracy of the simulations. The runner side spaces, radii at impeller and diffuser blades, and narrow gaps were not considered to obtain a computational grid with the highest possible quality (mostly block-structured grid). The impeller and diffuser were rebuilt and meshed using reverse engineering. Thus, the blade surfaces of the impeller and guide vanes could be extracted and used in a blade model tool for turbomachinery to modify the blade accordingly during the optimisation run. Vortex structures and dissipation were analysed within the transient calculations of the initial situation. The multi-stage centrifugal pump optimisation was mainly done in a simplified model to minimise the calculation effort. Impeller, inflow area and volute were optimised manually. Automated optimisation was realised for the guide vane and refeed channel. A multi-objective optimisation method based on an evolutionary algorithms was applied to a previously generated meta-model. An efficiency breakdown of the optimised two-stage pump geometry and a comparison with the original geometry were made as well. As a result of the optimisation, the efficiency is mainly increased in the entire operating range; in the single-stage variant by approx. 10%, and in the two-stage variant by approx. 7%! Hence the geometric specifications of the pump connection dimensions (retrofit) are adhered to, and the characteristic stability based on the CFD simulations is improved.

Keywords:
CFD, Multi-stage pump, Comparison of measurement and simulation

NOMENCLATURE

A	[m²]	Area
D	[m]	Diameter
g	[m/s²]	Gravity
Q	[m³/s]	Flow rate
H	[m]	Pump head
T	[Nm]	Torque
n	[rpm]	Rotational speed
NPSH	[m]	Net pressure suction head
n_q	[rpm]	Specific speed
p	[Pa]	Pressure
ρ	[kg/m³]	Density
φ	[-]	Flow coefficient
η	[-]	Efficiency
ψ	[-]	Pressure number

Subscripts and Superscripts, Abbreviations

BEP	Best efficiency point
SIC	Silicium carbide
GV	Guide vane
Histo	Histogram
IT	Intake (Suction side)
L	Loss
OT	Outtake (Pressure side)
RU	Runner
vap	Vapour
i	incipient
in	Inlet
hydr.	hydraulic
out	Outlet
stat	static
tot	total

1. INTRODUCTION

The HZ-type is a single- or multi-stage between bearings ring section centrifugal pump with shaft seal realised with radial split casing design.

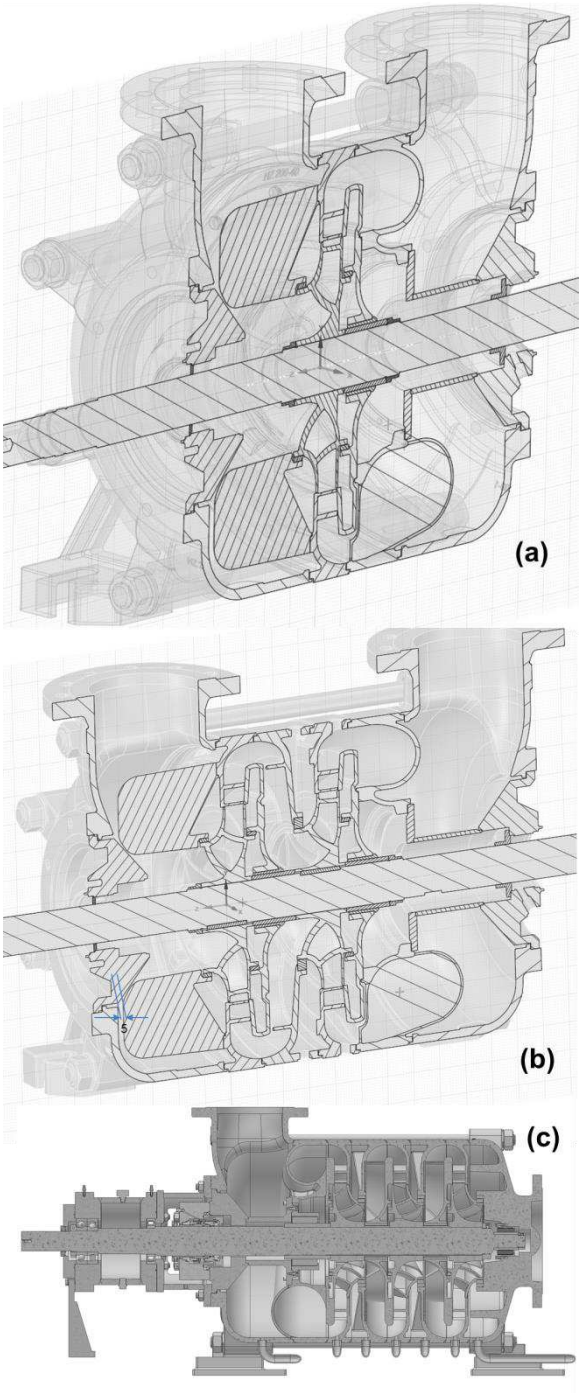

Figure 1. Single, double and multi stage arrangement

To achieve low NPSH values, the suction stand is designed as an inlet spiral or in axial direction. The suction side impeller is developed with an enlarged inlet cross-section (see Figure 1(a) for single, Figure 1(b) for double-stage and Figure 1(c) for multistage arrangement).

This series is applied in the industrial and municipal water supply, for the handling of condensates, boiler feed water, fuels, and other applications such as pressure boosting systems, boiler feed water, or condensate production.

The axial thrust compensation takes place through relief boreholes and throttle gaps. Suction, discharge and stage casings, as well as diffusers, are fitted with interchangeable wear rings as a standard.

The impellers are centred inside the diffusers. The diffusers are designed as fixed guide vane blade diffuser channels converting a part of the generated kinetic energy in the impeller into static pressure. The return vanes on the backside of the diffuser feed the pumped liquid to the impeller eye of the following stage. The closed impellers are hydraulically balanced through wear rings and balance holes in the impeller hubs. The pump is offered with axial and radial inlet. The bearings can be realised with roller bearings or slide bearings with oil lubrication (see example in Figure 1 (c), to be used on an oil platform in the North Sea..

2. NUMERICAL SIMULATION

2.1. Basics

The pump presented in this paper is designed for a stage-specific speed of n_q=36 rpm as a multi-stage pump. The specific speed n_q of the pump stage is calculated with Eq. (1) with the delivery head per stage.

$$n_q = n \cdot \frac{\sqrt{\frac{Q_{BEP}}{Q_{REF}}}}{\left(\frac{H_{BEP}}{H_{REF}}\right)^{0.75}} = 1480\ rpm \cdot \frac{\sqrt{\frac{0.13\ m^3/s}{1 m^3/s}}}{\left(\frac{35.6\ m}{1 m}\right)^{0.75}} = 35.9\ rpm \qquad (1)$$

Table 1. Nominal data of the pump

Speed	n	1480	rpm
Head	H_{BEP}	35.6	m
Discharge	Q_{BEP}	0.125	m³/s
Specific speed	$n_{q\_SingleStage}$	35.9	rpm
Efficiency	eta_{BEP}	0.73	%
Nominal Diameter	D_{out}	0.35	m
Pressure Number	$\psi_{BEP,Dout}$	0.978	-
Flow coefficient	$\varphi_{BEP,Dout}$	0.050	-

Similar to the applicable standard for turbine refurbishment [1], this paper follows the same procedure and first recalculates the existing initial geometry verified on the test rig and determines the potential for optimisation. For this purpose, the numerical calculation is compared with the test rig results using different models and considerable effort. Based on this initial situation, the optimisation is then carried out according to Figure 2. Based on a literature study [2]-[5] and a 1D

design on several streamlines, the first 3D model of the new hydraulic design was built utilising Ansys BladeGen®. A manual optimisation was performed for the impeller, the intake region, and the spiral area. For the elements of the guide vane (diffuser) and the return channel, an automated optimisation variant was applied.

2.2. Numerical models

An extracted fluid volume with many details is necessary to enable the highest possible accuracy of the simulations. The runner side spaces, radii at the impeller and diffuser blades (= guide vane), as well as narrow gaps were not taken into account to obtain a computational grid with the highest possible quality (most of the grid is block-structured). In addition, the extension on the inlet side and the outlet side was done by a straight pipe section with 10xD (D = 0.2 m) = 2 m each.

The impeller was rebuilt and meshed using "reverse engineering". Balancing holes were not included in the model.

Two models were generated and analysed before optimisation started. The single-stage model consists of 1 runner and 2 guide vanes (each as a 360° circular segment). The double-stage model consists of an additional return part with 8 blades after the guide vane and a second runner and second diffusor. Each model also includes a suction side and a spiral and outtake section with a full 360-degree model. Like the pressure side, this mesh was generated with ICEM®. In between, two stages are realised (see Figure 2).

The rotor now consists of 7 out of 7 passages for the impeller domain. The guide vane domain consists of 10 passages. The periodic boundaries of the impeller and diffusor domains have 1-to-1 interfaces, and Turbogrid® generates the mesh.

Table 2 itemises all important models with their overall mesh sizes. The HJCL mode of Turbogrid® follows an automated block topology depending on the blade metal angle, including full periodicity. In addition, it employs an algebraic, semi-isogeometric surface mesh generation procedure.

The commercial CFD code Ansys CFX V17.1 helped to solve the Navier-Stokes equations. These Navier-Stokes equations describe the fluid motion in all three dimensions and are applied for Reynolds averaged Navier-Stokes (RANS) formulation. RANS uses equations where – with the help of a Reynolds decomposition – the instantaneous variables are decomposed into mean and fluctuating values, whereas these variables are time-averaged.

For the stationary and single-phase CFD simulations, the frozen-rotor approach was used to model the transition from stationary calculation areas (suction area, guide vane) to the rotating calculation area (impeller) and vice versa. Five different positions impeller positions ("clocking") were analysed. In addition, the so-called mixing-plane interface model (stage) was also used. In this case, a circumferentially averaged velocity field is transmitted between the computational regions. Experience has shown that the stage interface provides more accurate results but is rather unstable, especially under unfavourable flow conditions.

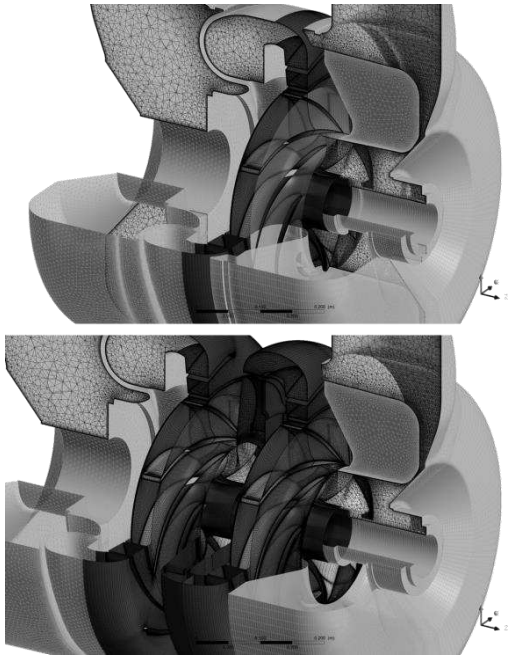

Figure 2. Models for CFD calculation, top - single-stage, bottom: double stage arrangement

At the inlet to the intake pipe, the mass flow and the inflow direction (free from swirl) are specified. At the outlet from the outlet pipe a constant static pressure was defined. The delivery head of the pump thus adjusts itself depending on the selected flow rate (mass flow) in the course of the CFD simulation.

Table 2. Model, mesh sizes in million

Standard model		Single stage		Double stage	
Domain	*# blades, info*	**Nodes**	**Elements**	**Nodes**	**Elements**
Intake		1.71	3.06	1.25	2.19
Runner1	*7/7*	2.20	2.08	2.20	2.08
Diffuser1	*10/10*	2.98	2.80	2.98	2.80
Rueck1	*8/8*			3.05	2.92
Runner2	*7/7*			2.20	2.08
Diffuser2	*10/10*	1.49	3.48	2.98	2.80
PressureEnd				1.49	3.48
All Domains		**8.38**	**11.42**	**15.95**	**17.96**

Optimisation model		fine		medium	
Domain	*# blades, info*	**nodes**	**elements**	**nodes**	**elements**
Intake	*"suction casing+ inlet pipe"*	0.60	0.56	0.39	0.36
Runner	*1/7*	0.38	0.74	0.18	0.32
Diffuser	*2/10*	0.03	0.06	0.14	0.30
PressureEnd	*"spiral+pressure pipe"*	0.32	0.30	0.20	0.18
All Domains		**1.55**	**2.19**	**0.91**	**1.17**

The SST model developed by Menter [6] was applied to stationary calculations as the turbulence model. Based on an Eddy-viscosity concept, this two-equation approach is commonly used for hydraulic turbomachinery combining the 2-

equations-turbulence-models k-ε- and k-ω. The transient analyses were carried out with the SAS-SST turbulence model by Menter. Although, using the SST turbulence model for transient simulations (URANS) could be an option. However, experience has shown that its application does not always provide satisfying results, even if the grid and time step resolution would be adequate. Hence, preference was given to the scale resolving turbulence model SAS-SST. The concept of the SAS turbulence model rests on the introduction of the Von Karman length scale into the turbulence scale equation [7]. The model dynamically adjusts to resolved vortex structures in the URANS (Unsteady Reynolds Averaged Navier Stokes) method, resulting in a LES-like (Large Eddy Simulation) behaviour in unsteady regions of the flow field. For the investigations and the transient simulations presented in this paper, the choice fell on the Shear-Stress-Transport turbulence model for Scale Adaptive Simulations (SST-SAS), combined with the Curvature Correction (CC) model developed by Smirnov and Menter and a production limiter model according to Kato-Launder.

2.3. Post-processing

The key figures mentioned in the following are of interest for evaluating hydraulic performance. In general, the net head is the difference between the total pressure at the outlet and the total pressure at the inlet. According to the standard ISO 9906 [8], the net head represents the difference between the inlet's and the outlet's static pressure. The mean kinetic energy head difference is added to the head (geodetic head difference neglected, see Eq. 2). The pressure was measured on the test rig on 4 pressure measuring taps displaced by 90° of each other, the locations being 2D away from the flange (Figure 3). Therefore, the post-processing of the CFD results was carried out similarly (Eq. 3).

$$H = \frac{1}{\rho g}\left[\left(\frac{1}{4}\sum_{i=1}^{4} p_i + \frac{\rho}{2}\left(\frac{Q}{A}\right)^2\right)\Big|_{Outlet} - \left(\frac{1}{4}\sum_{i=1}^{4} p_i + \frac{\rho}{2}\left(\frac{Q}{A}\right)^2\right)\Big|_{Inlet}\right] \quad (2)$$

$$H = \frac{1}{\rho g}\left[\frac{1}{A_{Outlet}}\left(\int p_{stat}\cdot dA\right)|_{Outlet} - \frac{1}{A_{Inlet}}\left(\int p_{stat}\cdot dA\right)|_{Inlet}\right] + \frac{\left(\frac{Q_{Outlet}}{A_{Outlet}}\right)^2 - \left(\frac{Q_{Inlet}}{A_{Inlet}}\right)^2}{2g} \quad (3)$$

The NPSH evaluation was carried out employing histogram analysis, which requires only a single phase calculation. This method was cross-checked several times [9,10]. The pressure $p_{Histogram}$ is the value when the pressure at a certain blade surface percentage exhibits pressure lower than the $p_{Histogram}$. The idea is that a single value for the minimum pressure is not real but happens in a numerical simulation. This pressure allows for the conventional calculation of the NPSH value within a single-phase calculation without a cavitation model. The area percentage representative for the pump type under investigation has to be known. However, this percentage changes from one pump type to the other. To determine the corresponding data is only possible by comparing a sufficiently large number of experimental and numerical results for different pump types. Reducing the area percentage results in a shift of the calculated NPSH value towards $NPSH_i$, by increasing it towards $NPSH_3$. Index 3 means a 3% drop of the delivery head per stage [8].

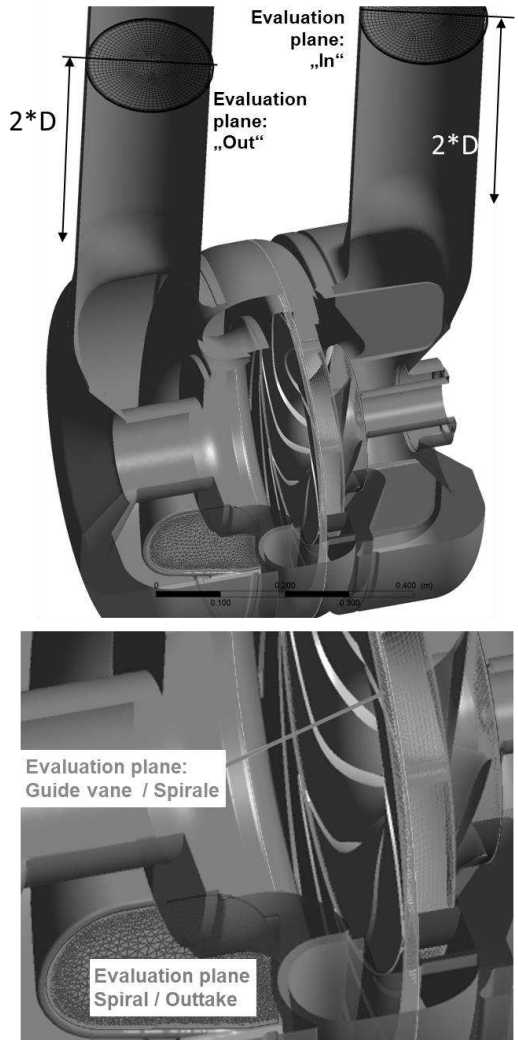

Figure 3. Evaluation planes CFD model

The efficiency is the benefit versus the expenditure and is described with Eq. 5. To analyse each component separately, a head loss analysis (see Eq. 6) was performed to calculate a cumulative distribution of the total unit. In this case, the total pressure difference between the inlet and outlet of each component was set in comparison to the net head. For the runner, the shaft power was also considered and added to the losses (Eq. 8).

$$NPSH = \frac{p_{tot,s} - p_v}{\rho \cdot g} = \frac{p_{tot,s} - p_{Histo}}{\rho \cdot g} \quad (4)$$

$$\eta_{hydr} = \frac{P_{hydr}}{P_{mech}} = \frac{\rho \cdot g \cdot Q \cdot H}{T_{Runner} \cdot \omega} = \frac{\rho \cdot g \cdot Q \cdot H}{(T_{Ru-Blades} + T_{Ru-Hub} + T_{Ru-Shroud}) \cdot \frac{2 \cdot \pi \cdot n}{60}} \quad (5)$$

$$\eta_{hydr} = \frac{H_{Pump}}{H_{Pump} + \sum H_{Loss}} = \frac{H_{Pump}}{H_{Pump} + H_{L-IT} + H_{L-Ru} + H_{L-GV} + \cdots + H_{L-OT}} \quad (6)$$

$$H = {}_{L-IT} = \frac{p_{Tot@In} - p_{Tot@Inlet-Runner}}{\rho \cdot g} \quad (7)$$

$$H_{L-Ru} = \frac{p_{Tot@Inlet-Ru} - p_{Tot@Ru-GV}}{\rho \cdot g} + \frac{T_{Ru} \cdot \omega}{\rho \cdot g \cdot Q} \quad (8)$$

$$H_{L-GV} = \frac{p_{Tot@Runner-Guidevane} - p_{Tot@Guidevane-Spiral}}{\rho \cdot g} \quad (9)$$

$$H_{L-Spiral} = \frac{p_{Tot@Guidevane-Spiral} - p_{Tot@Out}}{\rho \cdot g} \quad (10)$$

3. RESULTS OF EXISTING HYDRAULIC DESIGN

For comparison purposes concerning the measured data of the existing pump, the CFD simulations were calculated with different models for the rotor-stator interface. Figure 4 shows the result of the steady-state calculation with the frozen rotor and the stage interface. In addition, a transient calculation was also evaluated and compared with the existing measurement data. Finally, the data for the experimental test was extrapolated to full load.

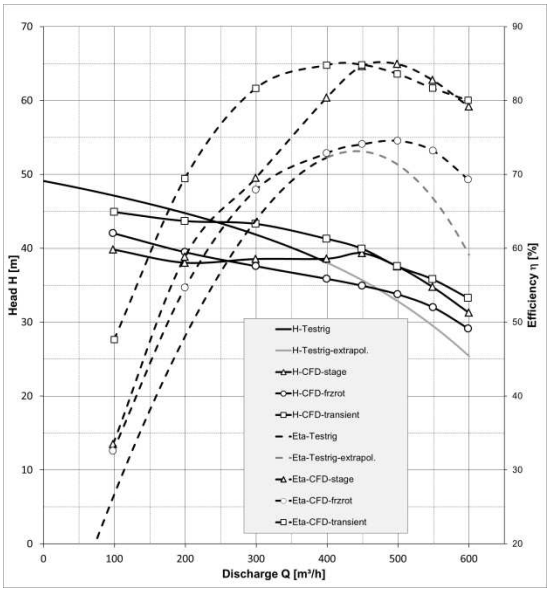

Figure 4. Single-stage, CFD vs test rig

The optimum position in the transient calculation is quite good in terms of discharge. The difference in efficiency is mainly due to the use of hydraulically smooth walls and the non-modelled impeller side spaces, leakage losses, and bearing losses

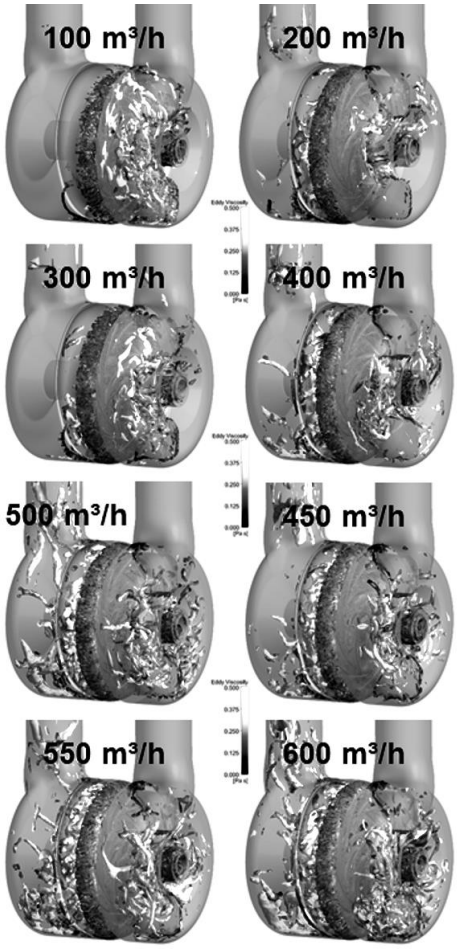

Figure 5. Q-criterion, single-stage, original geometry

At this point, Figure 5 shows an analysis of the existing vortex structures and their dissipation with the help of the Q-criterion shows a high dissipation rate in the suction area at the lowest flow rates and in the pressure area at the highest flow rates. The area of the guide vane, on the other hand, is filled with vortex structures whose intensity, however, is significantly lower. Figure 6 shows the efficiency splitting for the 2-stage case. This cumulative efficiency plot shows the individual components with their losses. One clearly sees the losses increasing from the optimum point in both directions to part and overload. In addition, the measurement result from the measurement of the 2-stage case from the test rig is shown, with the optimum points slightly shifted to overload for the measurement. The result of the cavitation measurement now indicates a somewhat different behaviour than that of the numerical simulation. The measured values are clearly below those of the numerical simulation, whereby the distance to full

load, the dimensioning variable, becomes visibly smaller and is equalised at 600m³/h in any case.

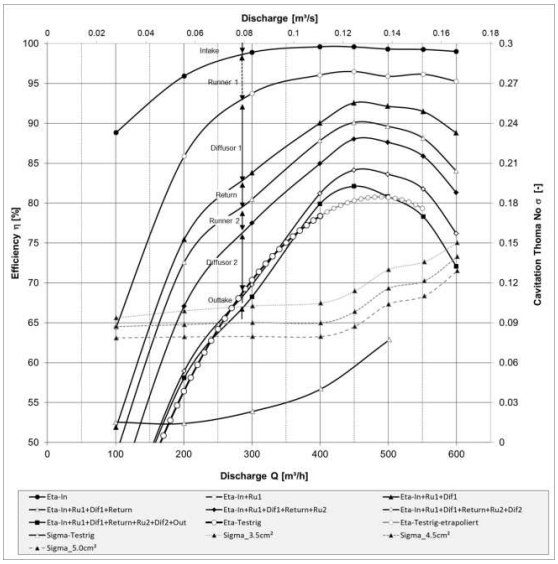

Figure 6. Double-stage, efficiency splitting

4. MODIFICATIONS

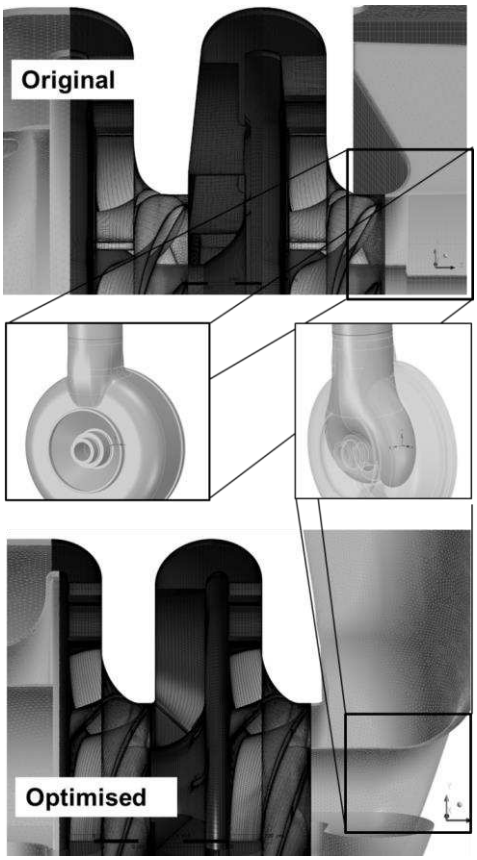

Figure 7. Modifications, top original, bottom optimised.

The optimisation of the suction area (Figure 7) also affects the improvement of the head curve stability. Still, a possible reduction in efficiency must also be taken into account. The spiral outlet was left at the lowest point for self-priming. Now 10 planar guide vanes and 8 curved return vanes are used, which are the result of the parametric optimisation model for the meridian and the shape of the blades. This model has about 50 geometric degrees of freedom. The outer diameter of the stage dramatically influences the head and efficiency at all the operating points studied (300, 400 and 500 m³/h), and it proves the more significant, the better.

The diameter of the trailing edge of the return vanes has a major influence on the head and efficiency of the downstream impeller. Here, it proves the smaller, the better. The length of the stage is not so decisive.

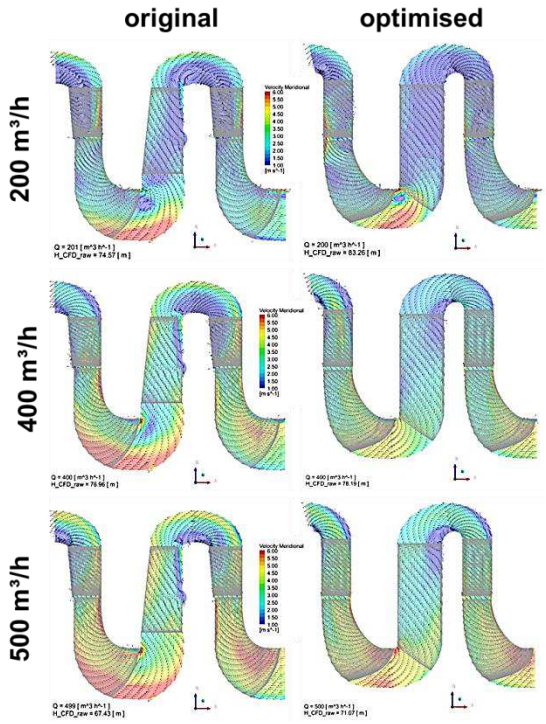

Figure 8 Modification of the guide vane

The velocity distribution in the meridian section at different operating points (at Q = 200 m³/h – top Q = 400 m³/h – centre; Q = 500 m³/h – bottom for the original geometry (left) and the optimised pump geometry (right) is illustrated in Figure 8, in which a reduction of areas with high velocities is present.

The distribution of the meridional component of the velocity (c_m – Figure 9) and the circumferential component (c_u – Figure 10) at Q = 450 m³/h are analysed at different positions in the pump for the original geometry (grey) and the optimised pump geometry (black).

Even a slight change in the shape of the blade (variation of the exit angle by +- 2°) can significantly change the shape of the characteristic curve and the position of the efficiency optimum with otherwise unchanged geometry (Figure 11).

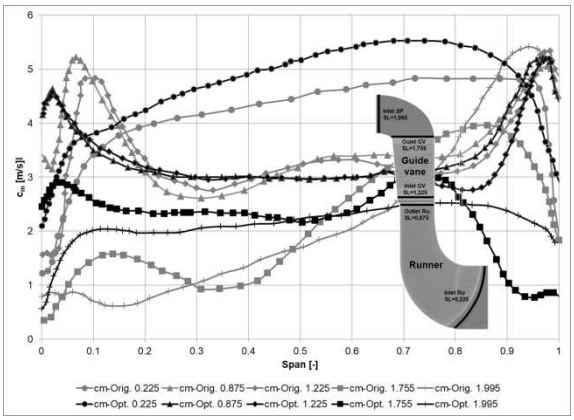

Figure 9. Meridional velocity at different locations

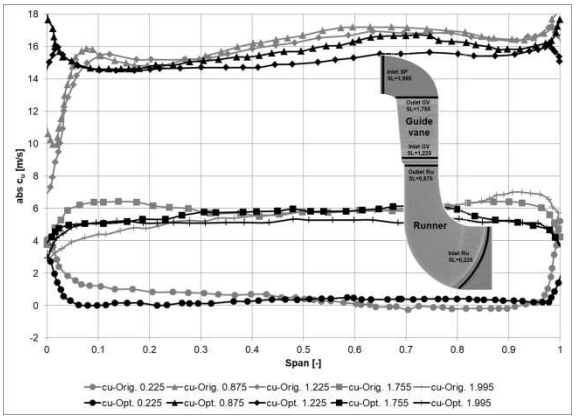

Figure 10. Circumferential velocity at different locations

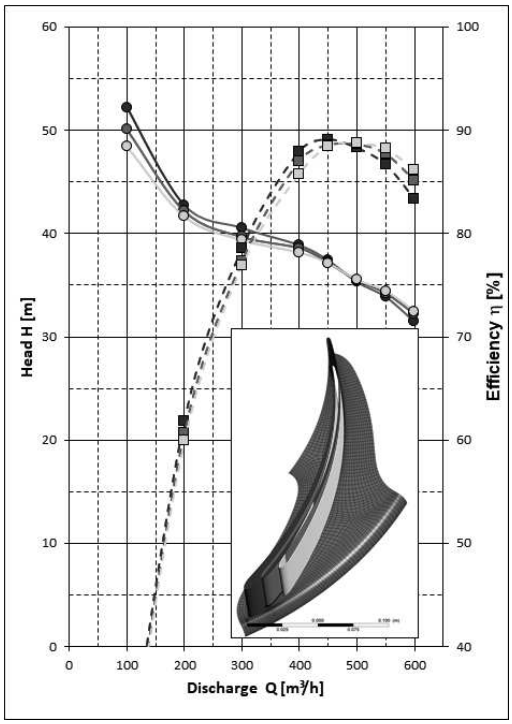

Figure 11 Modification of the guide vane

5. RESULTS OF THE OPTIMISED HYDRAULIC DESIGN

Comparing the initial geometry with the optimised variant in terms of efficiency shows each component's advantageousness and interaction. In the desired optimum of the pump at Q=450 m³/h, the efficiency could be increased by $\Delta\eta$=7%. Figure 12 shows the efficiency breakdown of the optimised pump geometry (1-stage) and a comparison with the original geometry (grey lines). An improvement of the flow situation (loss minimisation) can be observed in all components; most of the efficiency increase is due to the optimised guide vane. However, at 500 m³/h, there are already approx. 4% points of losses in the outtake! There may be further potential here.

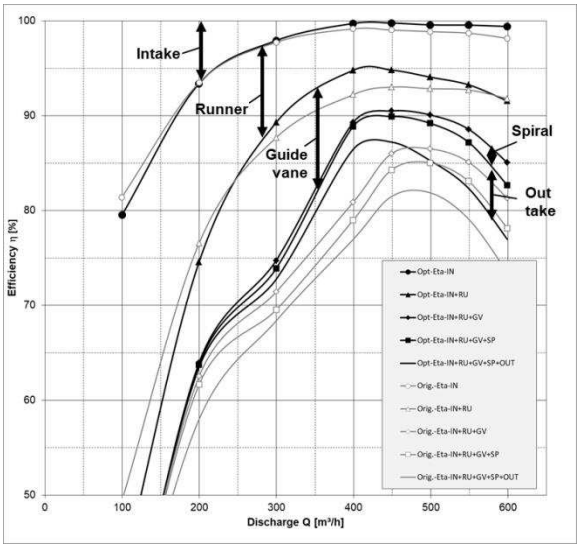

Figure 12. Single-stage, efficiency splitting, optimised versus original geometry

Figure 13 shows the comparison of the pump head curve determined through CFD simulation in the full model for the original pump geometry (black with circles) and the final optimisation variant (black with diamonds). The CFD simulation also shows a slight head curve bend (full load bend) of the final optimisation variant for the 2-stage version; original geometry also shows this behaviour. At 400 m³/h, the head could be increased by 4 m; the efficiency in the entire operating range between 300 m³/h and 600 m³/h by approximately 7 %. Like the transient calculation of the single-stage original geometry, the final transient calculation is above the steady-state results. The improvement of the cavitation behaviour is shown in the lower part of Figure 13. The increase after overload could be pushed to even higher flow rates. Finally, Figure 14 shows the flow situation at the pump-eye. For this purpose, $NPSH_{required}$ was plotted on the impeller walls to avoid falling below the vapour pressure.

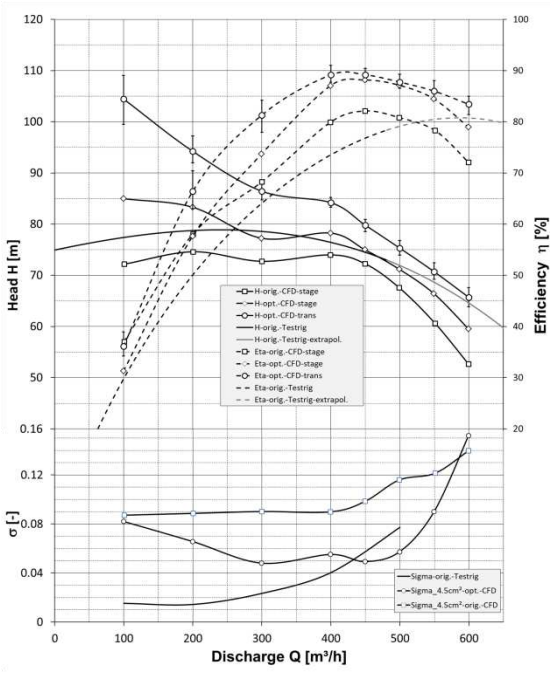

Figure 13. 2-stage optimised versus original geometry

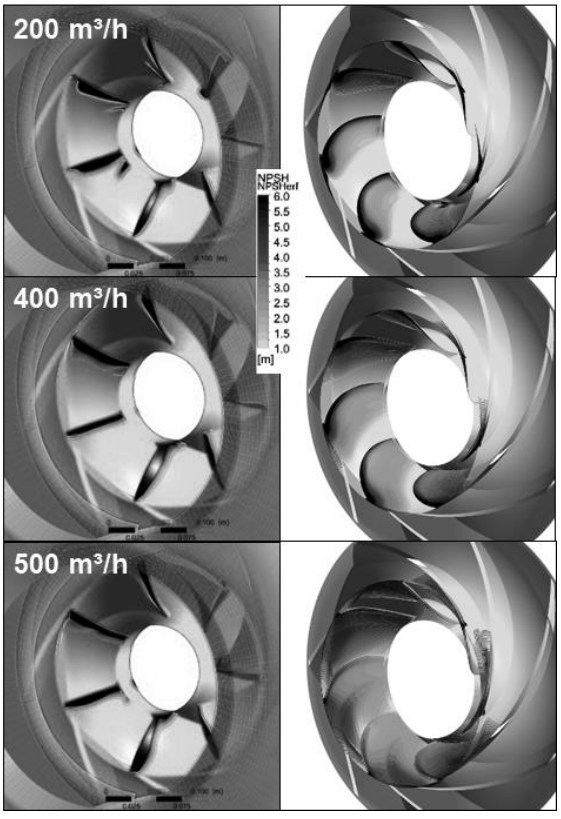

Figure 14. Runner inlet at different discharges, cavitation behaviour

The dark zones mean that 6 m of NPSH are necessary to prevent falling below the vapour pressure. Again, clearly pronounced zones can be found on the left side of the original geometry. In contrast, on the right side of the optimised variant, these are, if at all, significantly smaller.

6. CONCLUSION

For a pump series built in single- and multiple-stage design, a corresponding optimisation potential could be determined based on an extensive recalculation of the actual status. The individual components could be successively improved through a hybrid approach consisting of manual and automated optimisation. Thus, the efficiency in the entire operating range could be significantly increased. In the single-stage variant at Q = 400 m³/h by approx. 10% (!), two-stage in the entire operating range between 300 m³/h and 600 m³/h by approx. 7%! It was also possible to improve the characteristic stability based on the CFD simulations and increase the delivery head. Geometry specifications concerning retrofit could all be met.

REFERENCES

[1] International Electrotechnical Commission, IEC 62256:2017, Hydraulic turbines, storage pumps and pump-turbines – Rehabilitation and performance improvement.

[2] Stepanoff, A. J., 1959, Radial- und Axialpumpen, Springer.

[3] Guelich, J. F., 2004, Kreiselpumpen, Springer.

[4] Pfleiderer, C., Petermann, H., 2005, "Strömungs-maschinen", 7th Edition, ISBN 3-540-22173-5, Springer.

[5] Karassik, I, Messina, J. P., Cooper, P., Heald, C.C., 2001, "Pump Handbook", 3rd Edition, ISBN 0-07-0304032-3, McGraw-Hill.

[6] Menter, F. R., 1994, "Two-equation eddy-viscosity turbulence models for engineering applications", *AIAA Journal*, Vol. 32, pp.1598–1605.

[7] Menter, F. R., Egorov, Y., 2005, "A Scale-Adaptive Simulation Model Using Two-Equation Models", *AIAA Journal*., pp. 271–283

[8] International Standard ISO 9906:2012, Rotodynamic pumps – Hydraulic performance acceptance tests – Grades 1, 2 and 3.

[9] Gehrer, A., Benigni, H., Penninger, G., 2004, "Dimensioning and Simulation of Process Pumps," *Karlsruhe Pump Users Technical Forum*, Karlsruhe, Germany.

[10] Benigni, H., Jaberg, H., Yeung, H., Salisbury, T., Berry, O., 2012, „Numerical Simulation of Low Specific Speed API Pumps in Part-Load Operation and Comparison with Test Rig Results", In: Journal of fluids engineering 134 (2012) 2, pp. 024501-024501.